Springer

KSME

Journal of Mechanical Science and Technology 24 (11) (2010) 2161~2167
www.springerlink.com/content/1738-494x
DOI 10.1007/s12206-010-0510-5

Seven-bar mechanical press with hybrid-driven mechanism for deep drawing; Part 2: Dynamic modeling and simulation †

Hui Li* and Yuping Zhang

Department of Electromechanical Engineering, Shijiazhuang Institute of Railway Technology, Shijiazhuang 050041, P.R. China

(Manuscript Received April 6, 2009; Revised April 16, 2010; Accepted April 16, 2010)

Abstract

Modeling and dynamic analysis of the electromechanical coupling system of a hybrid-driven mechanical press were undertaken. A dynamic model of a two-degrees-of-freedom seven-bar linkage was developed using Lagrange's equation. According to the equivalent circuit of a DC motor and a brushless servomotor, a dynamic model and negative feed-back model were separately developed. The fourth-order Runge-Kutta method, an explicit method, was employed as the integration technique in a computer simulation, and the time history of the hybrid-driven press was obtained.

Keywords: Hybrid-driven mechanism; Press; Dynamics; Computer simulation; Mechatronics; Servomotor

1. Introduction

In traditional mechanical presses, the driving power, as transmitted to the drive shafts through a reducer device, usually is obtained from a constant-speed motor. However, this mechanism, though it can be designed to satisfy high-speed mass production, generally is considered to be too inflexible to meet the challenges posed by frequent changes in either manufacturing processes or products. Complex mechanistic methods that might provide this versatility sometimes become expensive or are difficult to achieve [1, 2]. Many researchers working to solve this dilemma have developed a flexible press, which uses a servomotor as the prime mover. However, a servomotor's power capacity usually is limited [3-6]. Recently, researchers looking for answers have turned to the hybrid-driven mechanism [7-20]. The main idea in the hybrid-driven concept is to combine the motion of a large constant-velocity motor with a small servomotor via a two-degrees-of-freedom mechanism. The constant-velocity motor provides the main power and motion requirement, while the servomotor acts as a low-power motion-modulation device. The hybrid-driven idea was studied initially by Tokuz and Jones [7-10]. In their investigations, inputs from a constant-speed motor and a servomotor were summed in a differential gearbox to produce non-uniform motion at the output of a linkage. The fundamental non-uniform motion requirement is derived from a linkage mechanism and the second input, which, being programmable, imparts the modulation to that fundamental motion. A dimensional synthesis of a hybrid-driven mechanical press suitable for deep drawing was completed in the present study's Part 1. Also, in Part 1, a method of optimizing the displacement trajectory of the servomotor was derived. This hybrid-driven mechanical press has the characteristics of an approximately constant working velocity and, accordingly, a quick return. Thus, by properly optimizing the displacement trajectory of the servomotor, the output motion of the slider can pass through the desired trajectories. Thereby, the hybrid-driven mechanical press is endowed with flexible output motion characteristics suitable for deep drawing. These characteristics also provide the advantages of applicability to materials of different thicknesses or with plastic deformations.

In the present, Part 2 study, the dynamics of the hybrid-driven press, as powered by a DC motor and a brushless servomotor, were studied by mathematical modeling and a simulation. Then, dynamic system equations were derived and solved numerically. The fourth-order Runge-Kutta method, an explicit method, was chosen as the integration technique in the computer simulation. The simulation results obtained were tabulated for a motion profile. In this paper, the simulation results are presented and discussed.

2. Mathematical model for hybrid-driven mechanical press system

2.1 Mathematical model for seven-bar linkage

A mathematical model for a seven-bar mechanism was de-

† This paper was recommended for publication in revised form by Associate Editor Hong Hee Yoo

* Corresponding author. Tel.: +86 311 88621089, Fax: +86 311 88621073
E-mail address: Huili68@163.com

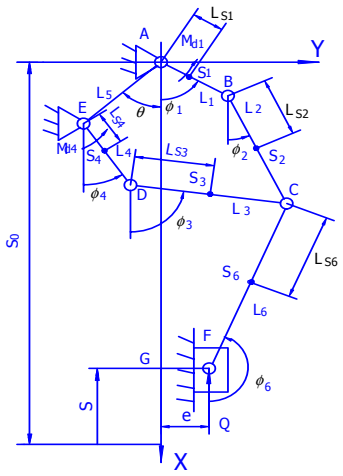

Fig. 1. Schematic representation of hybrid-driven press.

veloped using Lagrange's formulation. The system's equation of motion was derived with expressions for the system energy function and its partial and time derivatives with respect to the defined generalized coordinates. The mechanism operates in the vertical plane, accounting for the effects of gravity. Ideal running conditions were assumed for modeling and computational convenience. Motor loss effects were not included in the formulations.

Fig. 1 represents a hybrid-driven seven-bar mechanism, S_i denoting the center of mass of the ith link. The location of the center of mass of the ith link is indicated by L_{Si}. Using the input angles ϕ_1 and ϕ_4 as the generalized coordinates describing the motion of the two-degrees-of-freedom (two-DOF) seven-bar mechanism ($q_1=\phi_1, q_2=\phi_4$), Lagrange's equation can be given as

$$\frac{d}{dt}\left(\frac{\partial E}{\partial \dot{q}_k}\right)-\frac{\partial E}{\partial q_k}+\frac{\partial V}{\partial q_k}=Q_k \qquad (k=1,2) \tag{1}$$

where E is the kinetic energy, V is the potential energy, Q_k is the generalized torque on link 1 and link 4, and q_k is the generalized coordinate.

The kinetic energy can be expressed as

$$E=\sum_{\substack{i=1\\ i\neq 5}}^{7}\left[\frac{1}{2}m_i\left(\dot{x}_{Si}^2+\dot{y}_{Si}^2\right)+\frac{1}{2}J_i\dot{\phi}_i^2\right] \tag{2}$$

where $\dot{\phi}_i$ is the angular velocity of link i, and $\dot{x}_{Si}$ and $\dot{y}_{Si}$ are the x and y velocity components of its center of mass. Then, $\dot{\phi}_i$, $\dot{x}_{Si}$ and $\dot{y}_{Si}$ can be written as

$$\dot{\phi}_i=\frac{\partial \phi_i}{\partial q_1}\dot{q}_1+\frac{\partial \phi_i}{\partial q_2}\dot{q}_2 \tag{3}$$

$$\begin{cases}\dot{x}_{Si}=\dfrac{\partial x_{Si}}{\partial q_1}\dot{q}_1+\dfrac{\partial x_{Si}}{\partial q_2}\dot{q}_2\\ \dot{y}_{Si}=\dfrac{\partial y_{Si}}{\partial q_1}\dot{q}_1+\dfrac{\partial y_{Si}}{\partial q_2}\dot{q}_2\end{cases} \tag{4}$$

where ϕ_i represents the angular displacement of link i. By substituting Eqs. (3) and (4) into Eq. (1),

$$E=\frac{1}{2}J_{11}\dot{q}_1^{\,2}+J_{12}\dot{q}_1\dot{q}_2+\frac{1}{2}J_{22}\dot{q}_2^2 \tag{5}$$

where J_{11}', J_{12}', J_{22} are the equivalent moments of inertia of the two-DOF seven-bar mechanism. These relationships are further elucidated in the Appendix.

The potential energy of the mechanism can be expressed as

$$V=-m_1gx_{S1}-m_2gx_{S2}-m_3gx_{S3}-m_4gx_{S4}-m_6gx_{S6}-m_7g(S_0-S) \tag{6}$$

where m_i represents the mass of link i, g the gravity constant, x_{Si} the location of the centers of mass of link i in axis x, and S the displacement of the slider.

According to the principle of virtual work, the generalized torque Q_k can be given as

$$\begin{bmatrix}Q_1\\ Q_2\end{bmatrix}=\begin{bmatrix}M_{d1}+Q\dfrac{\partial S}{\partial q_1}\\ M_{d4}+Q\dfrac{\partial S}{\partial q_2}\end{bmatrix} \tag{7}$$

where M_{d1} is the external input torque on the crank L_1, M_{d4} is the external input torque on the crank L_4, and Q is the forming force of the slider.

Differentiating Eqs. (5) and (6) and substituting them into Eq. (1) yields

$$\begin{bmatrix}Q_1\\ Q_2\end{bmatrix}=\begin{bmatrix}J_{11}\ddot{q}_1+J_{12}\ddot{q}_2+\dfrac{1}{2}\dfrac{\partial J_{11}}{\partial q_1}\dot{q}_1^2+\dfrac{\partial J_{11}}{\partial q_2}\dot{q}_1\dot{q}_2+\left(\dfrac{\partial J_{12}}{\partial q_2}-\dfrac{1}{2}\dfrac{\partial J_{22}}{\partial q_1}\right)\dot{q}_2^2+\dfrac{\partial V}{\partial q_1}\\ J_{22}\ddot{q}_2+J_{12}\ddot{q}_1+\left(\dfrac{\partial J_{12}}{\partial q_1}-\dfrac{1}{2}\dfrac{\partial J_{11}}{\partial q_2}\right)\dot{q}_1^2+\dfrac{\partial J_{12}}{\partial q_1}\dot{q}_1\dot{q}_2+\dfrac{1}{2}\dfrac{\partial J_{22}}{\partial q_2}\dot{q}_2^{\,2}+\dfrac{\partial V}{\partial q_2}\end{bmatrix}. \tag{8}$$

This is a second-order, nonlinear differential equation system representing the mechanism motion by generalized coordinates q_1 and q_2. The intermediate derivation steps and the derivate terms can be found in [20].

Eq. (8), the coupled equations, can be transformed into

$$\begin{cases}\ddot{q}_1=A_0+A_{11}\dot{q}_1^2+A_{12}\dot{q}_1\dot{q}_2+A_{22}\dot{q}_2^2\\ \ddot{q}_2=B_0+B_{11}\dot{q}_1^2+B_{12}\dot{q}_1\dot{q}_2+B_{22}\dot{q}_2^2\end{cases} \tag{9}$$

where A_0, B_0, A_{11}, B_{11}, A_{12}, B_{12}, A_{22}, B_{22} are the coefficients of the second-order differential equation. These coefficients are given in the Appendix.

2.2 Mathematical model for DC motors

Fig. 2 shows a DC motor, including a geared speed-reducer having a gear ratio of

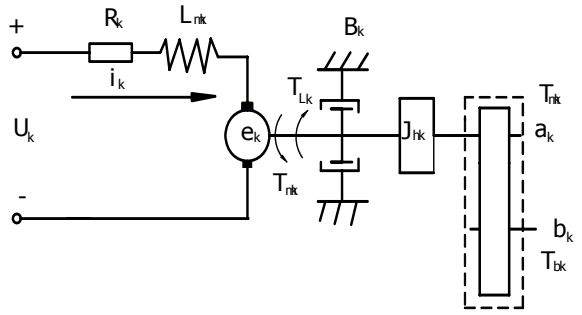

Fig. 2. Schematic representation of DC motor.

$$n_k = \frac{T_{bk}}{T_{ak}} = \frac{\omega_{ak}}{\omega_{bk}} \quad (k = 1, 2) \tag{10}$$

where ω_{ak} is the angular velocity of the input shaft a_k, and ω_{bk} is the angular velocity of output shaft b_k. In Fig. 2, the input to the motor-gear system is voltage U_k, and the output of the system is the torque T_{bk}, which, as defined in Eq. (7), is equal to M_{dk}. R_k, L_k, and i_k are the armature resistance, inductance and current, respectively. The shaft b_k is connected so as to drive the crank L_1 and crank L_4 of the mechanism, respectively. B_k is a damping coefficient due to a possible viscous bearing friction, T_{Lk} is a constant mechanical load, due to either brush friction, gear friction or dry bearing friction. J_{hk} is the combined moment of inertia of the motor rotor , the speed reducer, and the flywheel. Since two different DC motor types were studied, the same motor equations were used, and different motor data were utilized. Here, k is equal to 1 for a DC motor and 2 for a brushless servomotor, respectively, throughout the work. J_{hk} can be given as

$$J_{hk} = J_{mk} + J_{Rk} + J_{fk} \tag{11}$$

where J_{mk} is the moment of inertia of the motor rotor, J_{Rk} is the equivalent moment of inertia of the speed reducer, and J_{fk} is the moment of inertia of the flywheel.

From Kirchhoff's voltage law,

$$U_k = R_k i_k + L_{mk}\frac{di_i}{dt} + e_k \tag{12}$$

where e_k is the generated electromotive force of the motor.

Using a Newtonian equation for the mechanical load, we have

$$T_{bk} = n_k(T_{mk} - T_{Lk} - B_k\omega_{ak} - J_{hk}\frac{d\omega_{ak}}{dt}) \tag{13}$$

where T_{mk} is the magnetic motor torque, and n_k is the gear ratio defined by Eq. (10). The magnetic torque and the generated electromotive force are given as

$$T_{mk} = k_{tk} i_k \tag{14}$$

$$e_k = k_{ek}\omega_{ak} \tag{15}$$

where k_{tk} is the motor torque constant and k_{ek} is the motor voltage constant. Observing that

$$\omega_{ak} = n_k\omega_{bk} = n_k\dot{q}_k, \tag{16}$$

substituting Eqs. (14), (15) and (16) into Eqs. (12) and (13), we find

$$\frac{di_k}{dt} = \frac{U_k - R_k i_k - n_k k_{ek}\dot{q}_k}{L_{mk}} \tag{17}$$

$$T_{bk} = n_k k_{tk} i_k - n_k T_{Lk} - n_k^2 B_k\dot{q}_k - n_k^2 J_{hk}\ddot{q}_k, \tag{18}$$

Eqs. (17) and (18) being the mathematical models of the motor dynamics.

PID controllers are commonly used in many industrial processes. Their popularity is attributed partly to their performance in a wide range of operational conditions, and partly to their functional simplicity. Indeed, they can be operated by engineers in a simple and straight-forward manner. PID controllers utilize a control signal involving positional, velocity error and integral of position error functions. Here, the objective was to establish a PID control algorithm in order to determine how it can improve the transient and steady-state responses of the electromechanical system.

When the motor is controlled by the PID position closed loop, the voltage U_i can be given as

$$U_k = k_{pk}(q_{kic} - q_k) + k_{dk}(\dot{q}_{kic} - \dot{q}_k) + k_{Ik}\int_0^t (q_{Kc} - q_k)dt \tag{19}$$

where k_{pk} is the proportional gain constant, k_{dk} is the derivative gain constant, and k_{Ik} is the integral gain constant. q_{kc} and $\dot{q}_{kc}$ are the ideal angular displacement and ideal angular velocity of the crank L_k, respectively, and q_k and $\dot{q}_k$ are the actual angular displacement and actual angular velocity of the crank L_k, respectively.

Substituting Eq. (19) into Eq. (17),

$$\frac{di_k}{dt} = \frac{\left(k_{pk}(q_{kc} - q_k) + k_{dk}(\dot{q}_{kc} - \dot{q}_k) + k_{Ik}\int_0^t (q_{kic} - q_k)dt\right) - R_k i_k - n_k k_{ek}\dot{q}_k}{L_{mk}} \quad (k = 1, 2). \tag{20}$$

Eq. (20) is the PID control model of the servo motor dynamics. The proportional gain constant k_{pk}, the derivative gain constant k_{dk} and the integral gain constant k_{Ik} were optimized by running the simulation software with real mechanism parameters and motor data [17].

2.3 Mathematical model for electromechanical press system

Combining Eqs. (9) and (20) gives

$$\begin{cases} \ddot{q}_1 = A_0 + A_{11}\dot{q}_1^2 + A_{12}\dot{q}_1\dot{q}_2 + A_{22}\dot{q}_2^2 \\ \ddot{q}_2 = B_0 + B_{11}\dot{q}_1^2 + B_{12}\dot{q}_1\dot{q}_2 + B_{22}\dot{q}_2^2 \\ \dfrac{di_1}{dt} = \dfrac{\left(k_{p1}(q_{1c}-q_1) + k_{d1}(\dot{q}_{1c}-\dot{q}_1) + k_{I1}\int_0^t (q_{1c}-q_1)dt\right) - R_1 i_1 - n_1 k_{e1}\dot{q}_1}{L_{m1}} \\ \dfrac{di_2}{dt} = \dfrac{\left(k_{p2}(q_{2c}-q_2) + k_{d2}(\dot{q}_{2c}-\dot{q}_2) + k_{I2}\int_0^t (q_{2c}-q_2)dt\right) - R_2 i_2 - n_2 k_{e2}\dot{q}_2}{L_{m2}} \end{cases} \quad (21)$$

Let

$$x_1 = q_1, x_2 = q_2, x_3 = \dot{q}_1, x_4 = \dot{q}_2, x_5 = i_1, x_6 = i_2 ,$$

then Eq. (21) can be transformed into the system of first-order equations

$$\begin{cases} \dot{x}_1 = x_3 \\ \dot{x}_2 = x_4 \\ \dot{x}_3 = A_0 + A_{11}x_3^2 + A_{12}x_3x_4 + A_{22}x_4^2 \\ \dot{x}_4 = B_0 + B_{11}x_3^2 + B_{12}x_3x_4 + B_{22}x_4^2 \\ \dot{x}_5 = \dfrac{\left(k_{p1}(\phi_{1c}-x_1) + k_{d1}(\dot{\phi}_{1c}-x_3) + k_{I1}\int_0^t (\phi_{1c}-x_1)dt\right) - R_1 x_5 - n_1 k_{e1} x_3}{L_{m1}} \\ \dot{x}_6 = \dfrac{\left(k_{p2}(\phi_{4c}-x_2) + k_{d2}(\dot{\phi}_{4c}-x_4) + k_{I1}\int_0^t (\phi_{4c}-x_2)dt\right) - R_2 x_6 - n_2 k_{e2} x_4}{L_{m2}} \end{cases} \quad (22)$$

3. Simulation results and discussion

The dynamic behavior of this system was studied using numerical methods. The fourth-order Runge-Kutta method, an explicit method, was chosen as the integration technique; in fact, this is the commonly employed method for integration of a system of nonlinear equations. The motor current, the angular displacement and the angular velocity of the crank are treated as unknowns, and the time response of the motor-mechanism system is obtained by integrating the system of first-order equations through time.

The initial constant for the variables in Eq. (22) is zero. The motor and mechanism parameters of the hybrid-driven press are given in Table 1, Table 2 and Table 3. The gear ratios n_1 and n_2 defined in Eq. (10) are 75 and 60, respectively. The equivalent moment of inertia $J_{R1}+J_{f1}$ defined in Eq. (11) is equal to $50kgm^2$. The proportional gain constant and derivative gain constant are obtained by using optimization [20]. The optimum results were found to be $[k_{p1},k_{d1},k_{I1}]^T = [141.19,3.38,0]^T$ and $[k_{p2},k_{d2},k_{I2}]^T = [122.16,2.68,0]^T$, respectively. The motion cycle was 7.5 seconds and the simulation time was two motion cycles. The simulation time step was 2.083ms. The forming force of the press is given in Fig. 3. Since zero initial conditions are given for the motor current, the crank angle displacement and the crank angular velocity, transients were observed in the simulation results. The steady-state is then achieved in one motion cycle. Figs. 4(a), (b) and (c) show the simulation results for the crank L_1 (angular displacement, velocity, acceleration). The constant-speed motor rotates at 600 rpm and crank L_1 has 8 rpm at the end. Figs. 5(a), (b) and (c) show the simulation results for the crank L_4 (angular displacement, velocity, acceleration). Figs. 6(a), (b) and (c) show the simulation results for the slider (slider displacement, velocity and acceleration). The observation can be made, from Figs. 4(a), (b) and (c), that the output velocity, the acceleration response curve of the constant-speed motor, is regarded as oscillatory. This behavior, simply, is caused by the initial conditions being given as zero, along with the effect of the forming force. The tracking

Table 1. DC motor parameters.

DC motor model	$Z_4-180-21$
Rated power P_e	18.5 KW
Rated voltage U_e	440 V
Rated current I_e	52 A
Rated speed/maximum speed $n_e / n_{\max}$	600/1600 r/min
Moment of inertia GD^2	1.72 kg.m^2
Winding resistance R_1	0.973 Ω
Winding inductance L_{m1}	19.9×10^{-3} H
Motor voltage constant k_{e1}	6.2 V/rad/s
Motor torque constant k_{t1}	5.6627 Nm/A
Efficiency η	83.7%

Table 2. DC servo motor parameters.

Rated power P_e	3 KW
Maximum operating speed $n_{\max}$	3000 r/min
Rotor moment of inertia J_{m2}	6.8×10^{-4} kg.m^2
Winding resistance R_2	0.8Ω
Winding inductance L_{m2}	5.8×10^{-3} H
Motor voltage constant k_{e2}	0.8598 V/rad/s
Motor torque constant k_{t2}	0.76 Nm/A
Continuous stall torque T_e	10.2 Nm
Peak torque T_p	19.7 Nm

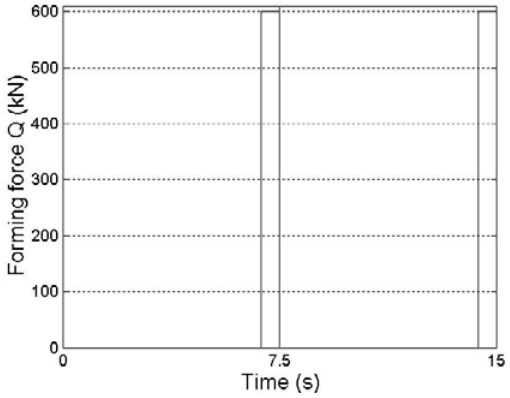

Fig. 3. Nominal capacity.

Table 3. Seven-bar mechanism parameters.

Parameters	Link 1	Link 2	Link 3	Link 4	Frame 5	Link 6	Slider 7
Link length L_i (mm)	161.089	674.046	673.62	114.166	509.678	1114.569	
Radius r_i (m)	0.025	0.025	0.025	0.025		0.025	0.025
Mass m_i (kg)	2.467	10.32	10.317	1.749		17.07	40
Moment of inertia J_i (kg.m^2)	0.0213	0.3909	0.3901	0.0076		1.7671	

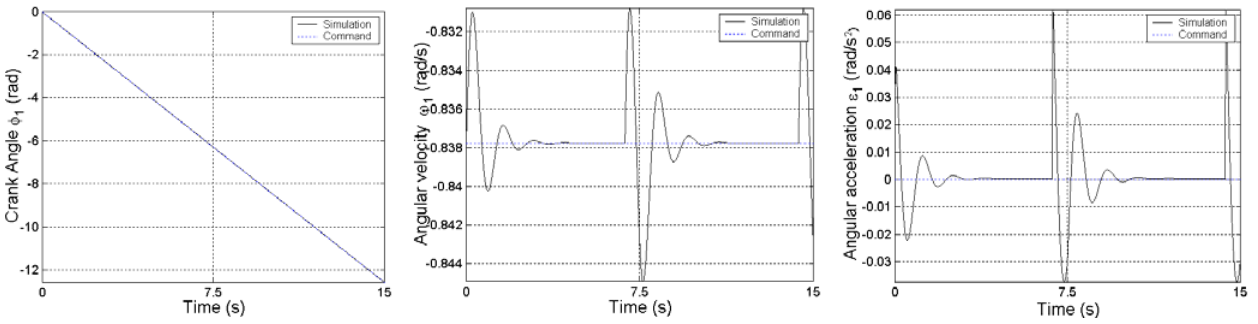

(a) Crank angle ϕ_1 (b) Angular velocity ω_1 (c) Angular acceleration ε_1

Fig. 4. Simulation results for crank L_1.

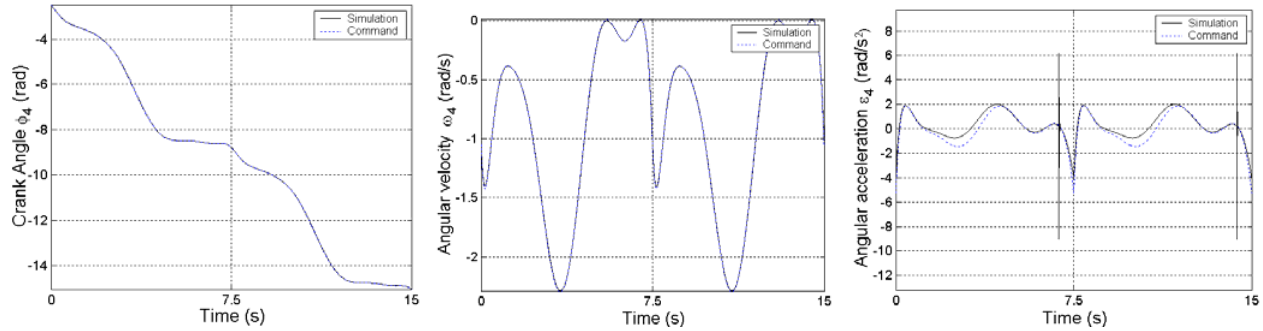

(a) Crank angle ϕ_4 (b)Angular velocity ω_4 (c) Angular acceleration ε_4

Fig. 5. Simulation results for crank L_4.

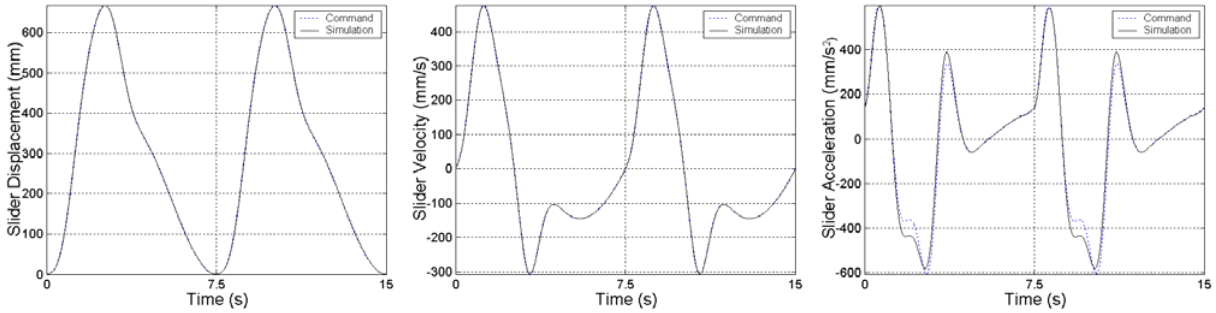

(a) Slider displacement (b) Slider velocity (c) Slider acceleration

Fig. 6. Simulation results for slider.

performance for the angular displacement, the velocity of crank L_4 driven by the servomotor, was very good in the first cycle. The simulation results for the slider were well correlated with the reference points.

4. Conclusions

In the present study, a theoretical investigation of a hybrid-driven press with its dynamics was undertaken, as discussed in this paper. Dynamic equations for the hybrid-driven press were derived and solved. The dynamic coupling of the electromechanical system, a highly non-linear problem, was revealed. Based on control theory, a PID controller of the hybrid-driven press was set up. The parameters of the controller were optimized by running simulation software with real mechanism parameters and motor data. The simulation was completed for an idealized system free from real effects. With these PID controller parameters, the steady-state was achieved within the first cycle. Better correlations between the simulated results and the given commands were obtained. Thus, theoretically and by computer simulation, the feasibility of the hybrid-driven press was verified.

Acknowledgments

The authors are grateful to the National Natural Science Foundation of China (No. 50775219 and No. 50975185), Zhejiang Provincial Natural Science Foundation (No. Y1080040). The authors are also grateful to the editors and reviewers for their constructive comments.

References

[1] D. He, *Crank presses,* China Machine Press, Beijing, China (1987).

[2] D. He, *Special presses,* China Machine Press, Beijing, China (1989).

[3] Yan Hongsen and Chen Weiren, A variable input speed approach for improving the output motion characteristics of watt-type presses, *International Journal of Machine Tools & Manufacture*, 40 (5) (2000) 675-690.

[4] S. Yossifon and R. Shivpuri, Analysis and comparison of selected rotary linkage drives for mechanical presses, *International Journal of Machine Tools & Manufacture*, 33 (2) (1993) 175-192.

[5] S. Yossifon and R. Shivpuri, Design considerations for the electric servo motor driven 30 ton double knuckle press for precision forming, *International Journal of Machine Tools & Manufacture*, 33 (2) (1993) 193-208.

[6] S. Yossifon and R. Shivpuri, Optimization of a double knuckle linkage drive with constant mechanical advantage for mechanical presses, *International Journal of Machine Tools & Manufacture*, 33 (2) (1993) 209-222.

[7] L. C. Tokuz and J. R. Jones, Programmable modulation of motion using hybrid machine, *Proceedings of Imeche*, C414/071 (1991)85-92.

[8] L. C. Tokuz, *Hybrid machine modeling and control,* Ph.D. Thesis, Department of Mech., Liverpool Polytechnic, UK (1992).

[9] L. C. Tokuz and J. R. Jones, Power transmission and flow in the hybrid machines, *The 6th International Machine Design and Production Conference*, Menu, Ankara, Turkey (1994) 209-218.

[10] L. C. Tokuz and J. R. Jones, A design guide for hybrid machine applications, *Transactions Journal of Engineering and Environment Sciences*, 21 (1997) 1-11.

[11] J. D. Greenough, et al., Design of hybrid machine, *Proceedings of the 9th IFToMM World Congress* (1995) 2501-2505.

[12] A. M. Conner et al., The synthesis of hybrid five-bar path generating mechanisms using genetic algorithms, *Genetic Algorithms in Engineering System: Innovations and Application* (1995) 313-318.

[13] Ali Kirecci and L.Canan Dulger, A study on a hybrid actuator, *Mechanism and Machine Theory*, 35 (8) (2000) 1141-1149.

[14] L. C. Dulger, Ali Kirecci and M. Topalbekiroglu, Modeling and simulation of a hybrid actuator, *Mechanism and Machine Theory*, 38 (5) (2003) 395-407.

[15] J. Herman, V. De Straete and J. De Schutter, Hybrid cam mechanism, *IEEE/ASME Transactions on Mechatronics*, 1 (4) (1996) 284-289.

[16] Bhartendu Seth and Sesha Sai Vaddi, Programmable function generators—1: base five-bar mechanism, *Mechanism and Machine Theory*, 38 (4) (2003) 321-330.

[17] Sesha Sai Vaddi and Bhartendu Seth, Programmable function generators — 2: seven-bar translatory-out mechanism, *Mechanism and Machine Theory*, 38 (4) (2003) 331-343.

[18] Hui Li and Ce Zhang, Research on the feasibility of hybrid-driven mechanical press, *Mechanical Science and Technology*, 23 (10) (2004) 1253-1256.

[19] Hui Li, Yuping Zhang, Haiqi Zheng, Dynamics modeling and simulation of a new nine-bar press with hybrid-driven mechanism, *Journal of Mechanical Science and Technology*, 22 (12) (2008) 2436-2444.

[20] Hui Li, *Fundamental study on the hybrid-driven programmable mechanical press*, Ph.D. Thesis, Tianjin University, Tianjin, China (2003).

Appendix

The kinetic energy E can be expressed as

$$E = \sum_{\substack{j=1 \\ j\neq 5}}^{7} \frac{1}{2}\left\{ m_j \left[\left(\frac{\partial x_{Sj}}{\partial q_1} \right)^2 + \left(\frac{\partial y_{Sj}}{\partial q_1} \right)^2 \right] + J_j \left(\frac{\partial \phi_j}{\partial q_1} \right)^2 \right\} \dot{q}_1^2 +$$

$$\sum_{\substack{j=1 \\ j\neq 5}}^{7} \frac{1}{2}\left\{ m_j \left[\left(\frac{\partial x_{Sj}}{\partial q_2} \right)^2 + \left(\frac{\partial y_{Sj}}{\partial q_2} \right)^2 \right] + J_j \left(\frac{\partial \phi_i}{\partial q_2} \right)^2 \right\} \dot{q}_2^2 +$$

$$\sum_{\substack{j=1 \\ j\neq 5}}^{7} \frac{1}{2}\left\{ m_j \left[\left(\frac{\partial x_{Sj}}{\partial q_1} \frac{\partial x_{Sj}}{\partial q_2} + \frac{\partial y_{Sj}}{\partial q_1} \frac{\partial y_{Sj}}{\partial q_2} \right) \right] + J_j \left(\frac{\partial \phi_j}{\partial q_1} \frac{\partial \phi_j}{\partial q_2} \right) \right\} \dot{q}_1 \dot{q}_2$$

where

$$J_{11}=\sum_{\substack{j=1\\ j\neq 5}}^{7}\left\{m_j\left[\left(\frac{\partial x_{Sj}}{\partial q_1}\right)^2+\left(\frac{\partial y_{Sj}}{\partial q_1}\right)^2\right]+J_j\left(\frac{\partial \phi_j}{\partial q_1}\right)^2\right\}$$

$$J_{12}=\sum_{\substack{j=1\\ j\neq 5}}^{7}\left\{m_j\left[\left(\frac{\partial x_{Sj}}{\partial q_1}\frac{\partial x_{Sj}}{\partial q_2}+\frac{\partial y_{Sj}}{\partial q_1}\frac{\partial y_{Sj}}{\partial q_2}\right)\right]+J_j\left(\frac{\partial \phi_j}{\partial q_1}\frac{\partial \phi_j}{\partial q_2}\right)\right\}$$

$$J_{22}=\sum_{\substack{j=1\\ j\neq 5}}^{7}\left\{m_j\left[\left(\frac{\partial x_{Sj}}{\partial q_2}\right)^2+\left(\frac{\partial y_{Sj}}{\partial q_2}\right)^2\right]+J_j\left(\frac{\partial \phi_i}{\partial q_2}\right)^2\right\}.$$

Explicit forms of A_0, B_0, A_{11}, B_{11}, A_{12}, B_{12}, A_{22}, B_{22} are given as

$$A_0=(Q_1J_{22}-Q_2J_{12})/C_1$$

$$B_0=(Q_2J_{11}-Q_1J_{12})/C_1$$

$$C_1=J_{11}J_{22}-J_{12}^2$$

$$A_{11}=\left[J_{12}\frac{\partial J_{12}}{\partial q_1}-\frac{1}{2}J_{12}\frac{\partial J_{11}}{\partial q_2}-\frac{1}{2}J_{22}\frac{\partial J_{11}}{\partial q_1}\right]\frac{1}{C_1}$$

$$B_{11}=\left[-J_{11}\frac{\partial J_{12}}{\partial q_1}+\frac{1}{2}J_{12}\frac{\partial J_{11}}{\partial q_1}+\frac{1}{2}J_{11}\frac{\partial J_{11}}{\partial q_2}\right]\frac{1}{C_1}$$

$$A_{12}=\left[J_{12}\frac{\partial J_{22}}{\partial q_1}-J_{22}\frac{\partial J_{11}}{\partial q_2}\right]\frac{1}{C_1}$$

$$B_{12}=\left[J_{12}\frac{\partial J_{11}}{\partial q_2}-J_{11}\frac{\partial J_{22}}{\partial q_1}\right]\frac{1}{C_1}$$

$$A_{22}=\left[\frac{1}{2}J_{12}\frac{\partial J_{22}}{\partial q_2}-J_{22}\frac{\partial J_{12}}{\partial q_2}+\frac{1}{2}J_{22}\frac{\partial J_{22}}{\partial q_1}\right]\frac{1}{C_1}$$

$$B_{22}=\left[-\frac{1}{2}J_{12}\frac{\partial J_{22}}{\partial q_1}+J_{12}\frac{\partial J_{12}}{\partial q_2}-\frac{1}{2}J_{11}\frac{\partial J_{22}}{\partial q_2}\right]\frac{1}{C_1}.$$

Hui Li received his B.S. in Mechanical Engineering from the Hebei Polytechnic University, Hebei, China, in 1991. He received his M.S. in Mechanical Engineering from the Harbin University of Science and Technology, Heilongjiang, China, in 1994. He received his PhD from the School of Mechanical Engineering of Tianjin University, Tianjin, China, in 2003. He was a postdoctoral researcher at Shijiazhuang Mechanical Engineering College from August 2003 to September 2005, and at Beijing Jiaotong University from March 2006 to December 2008. He is currently a professor in Mechanical Engineering at Shijiazhuang Institute of Railway Technology, China. His research and teaching interests include hybrid-driven mechanisms, kinematics and dynamics of machinery, mechatronics, CAD/CAPP, signal processing for machine health monitoring, diagnosis and prognosis. He is currently a senior member of the Chinese Society of Mechanical Engineering.